Natural Convection in a Quadrantal Cavity Heated and Cooled on Adjacent Walls

Orhan Aydin[1]
e-mail: oaydin@ktu.edu.tr

Gurkan Yesiloz

Department of Mechanical Engineering,
Karadeniz Technical University,
61080 Trabzon, Turkey

In this study, experimental and numerical analyses of natural convection in a quadrantal cavity heated and cooled on adjacent walls have been made to examine heat and fluid flow. Experimental studies involve the use of the particle tracing method that enables us to visualize the flow pattern in the enclosure. Numerical solutions are obtained using a commercial computational fluid dynamics package, FLUENT, using the finite volume method. Water is used as the working fluid. Effects of the Rayleigh number, Ra, on the Nusselt number, Nu, as well as velocity and temperature fields are investigated for the range of Ra from 10^3 to 10^7. A new approach is suggested to overcome the singularity at the corner joining the differentially heated isothermal walls when determining Nu. This novel approach is justified through the purely analytical conduction solution. The experimental and numerical results are shown to agree fairly well. Finally, a correlation for Nu is developed. [DOI: 10.1115/1.4003044]

Keywords: natural convection, quadrantal cavity, particle tracing method, singularity

1 Introduction

Natural convection phenomena in enclosures filled with fluids have been an interesting research topic in recent decades since they play a vital role in many engineering applications. Application areas include solar energy collection, nuclear energy, cooling of electronic components, microelectromechanical systems (MEMS), lubricating grooves, etc. Besides its importance in such processes, due to the coupling of fluid flow and energy transport, the phenomenon of natural convection remains an interesting field of investigation.

The existing literature presents a vast number of studies on natural convection in enclosures. However, most of these studies have been related to either a vertically or a horizontally imposed heat flux or temperature difference. There is little work regarding natural convection in enclosures with differentially heated neighboring horizontal and vertical walls. November and Nansteel [1] performed a numerical study on steady natural convection in a square water-filled enclosure heated from below and cooled from the adjacent wall. Ganzarolli and Milanez [2] numerically simulated steady natural convection in an enclosure heated from below and symmetrically cooled from the sides. Aydin et al. [3] studied the effect of aspect ratio on convection flow in a rectangular enclosure heated from one side and cooled from above. Aydin et al. [4] investigated the effects of inclination angle and Rayleigh number Ra on fluid flow and heat transfer characteristics for a two-dimensional square enclosure heated and cooled on adjacent walls. Aydin and Yang [5] numerically studied localized heating from below and symmetrical cooling from the sides. Angirasa et al. [6] reported a numerical study of buoyancy-driven transport from an isothermal symmetrically heated L-shaped corner. They discussed the effect of the length of the heated surface. Chinnakotla et al. [7] conducted a numerical study of buoyancy-induced flow and heat transfer over L-shaped corners with asymmetric heating. They maintained the horizontal and vertical surfaces isothermally with different temperatures, which are above the ambient temperature. Angirasa and Mahajan [8] studied natural convection fluid flow and heat transfer from L-shaped corners. In the study, the vertical side is hot and the horizontal side is either adiabatic or cold. The aspect ratio effect was studied in depth. Corvaro and Paroncini [9] analyzed natural convection in square cavities heated with a discrete heater from below and cooled by sidewalls. An experimental and numerical study on a vertical rectangular enclosure model with symmetrically localized heating and cooling zones was conducted by Ishihara et al. [10].

On the other hand, a great number of studies existing in the literature have been carried out for simple square and rectangular enclosures. As Shiina et al. [11] reported, those investigations do not serve us to determine natural convection in real enclosures with more complex geometries such as building systems with complex geometries and energy systems. They studied natural convection in a hemisphere heated from below. In another study, Chen and Cheng [12] performed a numerical and experimental study on natural convection inside an inclined arc-shaped enclosure. They emphasized that irregular-shaped enclosures had not been sufficiently analyzed yet despite the fact that they have relevance to some engineering applications such as concentrating solar collectors, lubrication systems, and air-conditioning devices. Kim et al. [13] studied steady-state natural convection in a meniscus-shaped cavity.

It should be also noted that many of the studies in the open literature are numerical only. In many of these studies, similar geometries are investigated very easily, which are too far from the interest of the practice. In addition, sometimes, additional effects are included in these studies, whose results are to be validated through analytical, if available, or experimental studies. However, there is a scarcity of experimental research when compared to an enormous number of theoretical ones.

The aim of the present study is to investigate experimentally and numerically the buoyancy-induced flow and heat transfer mechanisms in a water-filled quadrantal cavity when the lower surface of the cavity is heated while the vertical wall is cooled. The remaining curved wall is kept adiabatic. To the best knowledge of the authors, this is the first natural convection study on this geometry.

[1]Corresponding author.

Contributed by the Heat Transfer Division of ASME for publication in the JOURNAL OF HEAT TRANSFER. Manuscript received March 1, 2010; final manuscript received September 23, 2010; published online February 1, 2011. Assoc. Editor: Oronzio Manca.

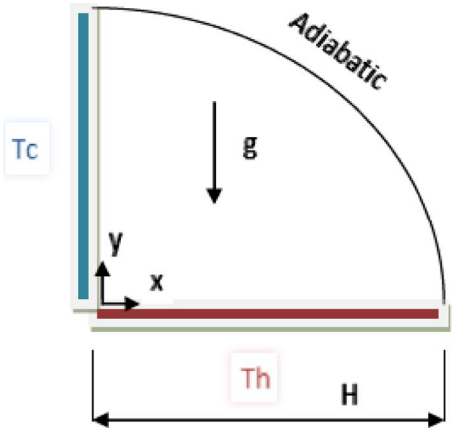

Fig. 1 Definition of the problem

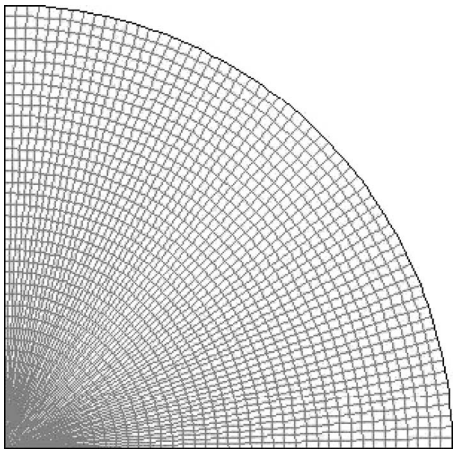

Fig. 2 Grid model

2 Numerical Study

In the present study, buoyancy-induced flow in a quadrantal cavity is isothermally heated from below and cooled by the vertical wall at uniform temperatures of T_h and T_c, respectively. The other curved wall is insulated. The schematic of the problem studied with the coordinates and boundary conditions is shown in Fig. 1.

All the walls are impermeable. The flow is assumed to be steady and laminar. Constant fluid properties are assumed, except for the density changes with temperature that induce buoyancy forces, so the Boussinesq approximation is adopted.

2.1 Governing Equations. The dimensionless form of the governing equations can be obtained via introducing dimensionless variables. These are defined as follows:

$$X=\frac{x}{H},\quad Y=\frac{y}{H},\quad U=\frac{u}{\alpha/H},\quad V=\frac{v}{\alpha/H},\quad P=\frac{pH^2}{\rho\alpha^2},\quad \theta=\frac{T-T_c}{T_h-T_c} \tag{1}$$

where u and v are the velocity components in the x- and y-directions, and T is the temperature. ρ and α are the density and the thermal diffusivity of the fluid, respectively. Based on the dimensionless variables defined in Eq. (1), the nondimensional equations for the conservation of mass, momentum, and energy equations are

$$\frac{\partial U}{\partial X}+\frac{\partial V}{\partial Y}=0 \tag{2}$$

$$U\frac{\partial U}{\partial X}+V\frac{\partial U}{\partial Y}=-\frac{\partial P}{\partial X}+\mathrm{Pr}\left(\frac{\partial^2 U}{\partial X^2}+\frac{\partial^2 U}{\partial Y^2}\right) \tag{3}$$

$$U\frac{\partial V}{\partial X}+V\frac{\partial V}{\partial Y}=-\frac{\partial P}{\partial Y}+\mathrm{Pr}\left(\frac{\partial^2 V}{\partial X^2}+\frac{\partial^2 V}{\partial Y^2}\right)+\mathrm{RaPr}\theta \tag{4}$$

$$U\frac{\partial \theta}{\partial X}+V\frac{\partial \theta}{\partial Y}=\frac{\partial^2 \theta}{\partial X^2}+\frac{\partial^2 \theta}{\partial Y^2} \tag{5}$$

Appearing in Eqs. (3) and (4), Pr and Ra are the Prandtl and Rayleigh numbers, respectively, which are defined as

$$\mathrm{Pr}=\frac{\upsilon}{\alpha},\quad \mathrm{Ra}=\frac{g\beta H^3(T_h-T_c)}{\upsilon\alpha} \tag{6}$$

where β and υ are the thermal expansion coefficient and the kinematic viscosity of the fluid, respectively. Through the introduction of the nondimensional parameters into the physical boundary conditions illustrated in Fig. 1, the following nondimensional boundary conditions are obtained:

$$\theta=1,\quad \mathrm{U=V=0}\quad \text{at}\quad \mathrm{Y=0}\quad \text{and}\quad 0<\mathrm{X}<1\quad \text{(on the bottom wall)} \tag{7}$$

$$\theta=0,\quad \mathrm{U=V=0}\quad \text{at}\quad \mathrm{X=0}\quad \text{and}\quad 0<\mathrm{Y}<1\quad \text{(on the vertical wall)} \tag{8}$$

$$\partial\theta/\partial\mathrm{X}=0,\quad \mathrm{U=V=0}\quad \text{at}\quad 0<\mathrm{X}<1\quad \text{and}\quad 0<\mathrm{Y}<1\quad \text{(on the adiabatic wall)} \tag{9}$$

2.2 Numerical Method. The numerical solution is obtained using a commercial computational fluid dynamics (CFD) software, FLUENT, which employs a finite volume method for the discretization of the continuity, momentum, and energy equations. The pressure-based solver is adopted, which was developed for low-speed incompressible flows. Owing to this technique the governing equations are solved sequentially (i.e., segregated from one another). Because the governing equations are nonlinear and coupled, the solution loop must be carried out iteratively in order to obtain a converged numerical solution. The SIMPLE algorithm is used to couple the pressure and velocity terms. Discretization of the momentum and energy equations is performed by a second order upwind scheme, and pressure interpolation is provided by the PRESTO scheme. The explanations of these algorithms can be found in the FLUENT User's Guide [14]. Convergence criterion is admitted at 10^{-5} for momentum and continuity equations, and for the energy equation it is lower than 10^{-12}.

2.3 Mesh Structure. Numerical studies in the existing literature suggest that the mesh system must be selected suitable to the specified problem. Mesh structure is one of the important parameters to obtain the correct solutions. In the literature, different approaches have been used to obtain mesh-independent solutions. In this study, the mesh is structured in such a way that the path of the heatlines, which intersect the isotherms spanning orthogonally from the isothermal hot bottom wall to the isothermal cold sidewall for the conduction solution given below, is considered. As will be shown below, the mesh structure used is also a mean overcoming the singularity at the corner.

The mesh model used is shown in Fig. 2. In the study, four different mesh sizes are adopted in order to check the mesh independence. A detailed grid independence study has been performed, and results are obtained for the average Nusselt number, the maximum values of the stream function, and the velocity magnitude in the enclosure. For example, at $\mathrm{Ra}=1.7\times10^5$ and $\mathrm{Pr}=6.62$, significant changes have not been observed between the

Table 1 Relative error analysis with different grid sizes

Grid	40×40	60×60	80×80	100×100
Nu	3.1932	3.1794	3.1592	3.155
Relative error (%)	0.432	0.635		0.133
Ψ_{max}	21.1742	21.1040	21.0805	21.0712
Relative error (%)	0.332	0.111		0.0441
V_{max}	128.0426	128.5909	128.6808	128.7722
Relative error (%)	0.426	0.0699		0.0709

grid sizes of 80×80 and 100×100. The difference in Nusselt number is 0.13% between these grid sizes. In this study, mesh refinement near the walls were also tested, but any considerable changes were not obtained. Thus, a uniform mesh size of 80×80 is adopted for the solutions (see Table 1).

2.4 Conduction Solution. For lower values of Ra, conduction is the dominant mechanism of heat transfer. Therefore, finding a conduction solution will also serve to validate the methodology followed. Assuming that there is no fluid motion, we consider energy transport occurring only by conduction. Because of the geometry of the problem, we use the cylindrical coordinate system at this point, which also helps to overcome the singularity at the corner, as shown in the following section. The energy equation in cylindrical coordinates can be written as

$$\frac{\partial^2 T}{\partial r^2}+\frac{1}{r}\frac{\partial T}{\partial r}+\frac{1}{r^2}\frac{\partial^2 T}{\partial \phi^2}=0 \tag{10}$$

which includes the radial, angular, and axial components of the heat flux given in the following:

$$q_r''=-k\frac{\partial T}{\partial r},\quad q_\phi''=-\frac{k}{r}\frac{\partial T}{\partial \phi} \tag{11}$$

The fact that there is no heat transfer at the radial direction and that the enclosure is two-dimensional, Eq. (10) will be reduced to

$$\frac{\partial^2 T}{\partial \phi^2}=0 \tag{12}$$

which means

$$\frac{\partial T}{\partial \phi}=\text{const} \tag{13}$$

The thermal boundary conditions are given as follows:

$$\phi=0,\quad T=T_h$$

$$\phi=\pi/2,\quad T=T_c \tag{14}$$

Solving Eq. (13) under the boundary conditions given in Eq. (14), we obtain the analytical conduction solution as

$$T=\frac{T_h-T_c}{\pi/2}\phi+T_h \tag{15}$$

which gives the angular variation in the temperature distribution. The isotherms representing the conduction solution are shown in Fig. 3. As seen, isotherms locate symmetrically from the hot wall to the cold wall.

2.5 Nusselt Number. The usual way of obtaining the Nusselt number at the isothermal walls requires temperature gradients at the surface normal of these walls. Keeping the adjacent walls at different temperatures causes the temperature discontinuity at the intersection of the hot and cold walls [3]. Due to the nonintegrable singularity of heat flux at this point, the total heat transfer is infinite. About this singular point, adopting some considerations is needed. The simplest way of handling this problem is assuming the average temperature of the two walls at the corner and keeping the adjacent nodes with the respective wall temperatures. Ganzarolli and Milanez [2] assumed a linear temperature profile between the corner node and the next adjacent node and performed some tests to determine the grid dependence of the average Nusselt number. Even though their tests showed that the grid dependence of the average Nusselt number is important for very coarse meshes only, the grid dependence of the local Nusselt number at this corner is very significant. The local Nusselt number very near this corner becomes larger and larger as the grid is refined. This can be clearly explained using the conduction solution shown in Fig. 3. As is shown, the limit of the temperature gradient either at the hot wall or at the cold wall approaches infinity when x or y goes to zero (i.e., the singular point). In fact, this is not very meaningful as far as the real physical systems are considered [3]. Note that the temperature discontinuity at this corner has no influence on the reliable numerical calculation of the interior velocity and temperature fields. However, from the practical viewpoint, it is critically necessary to make some considerations about the Nusselt number in order to obtain mesh-independent Nu solutions.

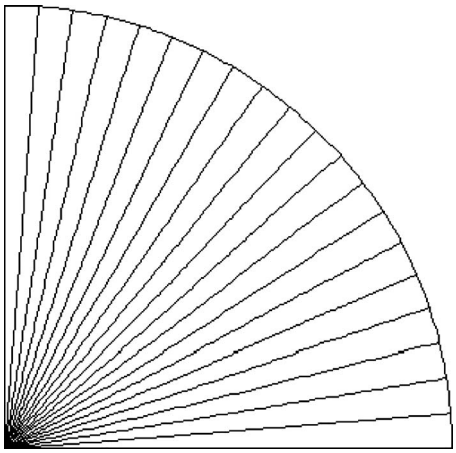

Fig. 3 Pure conduction solution

Taking all the above into consideration, this paper follows a new and reasonable approach for Nu calculation, which considers the paths of heatlines. Heat transfer occurs from a hot surface to a cold surface, following the path of these heatlines that intersect the isotherms perpendicularly. Accordingly, as we note above, the mesh structure chosen must be relevant to this definition for a reliable, cost-effective, and time-efficient solution. Therefore, the mesh system is structured by considering the conduction solution, which we strongly suggest for future convection heat transfer studies. The problem in the calculation of the Nusselt number regarding the Cartesian system can be overcome easily using the cylindrical coordinate system (r,ϕ). For the isothermal hot wall, the energy balance can be written as follows:

$$q_\phi''=-\frac{k}{r}\frac{\partial T}{\partial \phi}=h_r(T_h-T_c) \tag{16}$$

where h_r is the local heat convection coefficient. Using the conduction solution (Eq. (15)), the heat flux at the angular direction is defined as given below,

$$q_\phi''=\frac{k}{r}\frac{T_h-T_c}{\pi/2}=h_r(T_h-T_c) \tag{17}$$

Thus,

$$h_r=\frac{k}{r}\frac{1}{\pi/2} \tag{18}$$

is determined. Using Eq. (12), the Nusselt number is calculated as follows:

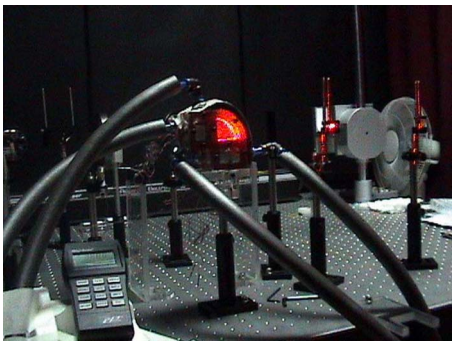

Fig. 4 Experimental setup

$$\mathrm{Nu}_r = \frac{h_r \cdot r}{k} \cdot \frac{\pi}{2} = \frac{k}{r} \cdot \frac{1}{\pi/2} \cdot \frac{r}{k} \cdot \frac{\pi}{2} = 1 \tag{19}$$

As is seen, Nu is equal to 1 for the conduction solution. Therefore, this result shows that heat is transferred only by conduction, and the correctness of the calculation procedure is approved.

Consequently, the Nusselt number along the heated wall can be defined as

$$\mathrm{Nu}_r = -\left.\frac{dT}{d\phi}\right|_{\phi=0} \cdot \frac{1}{T_h - T_c} \cdot \frac{\pi}{2} \tag{20}$$

3 Experimental Apparatus and Procedure

The photograph and the schematic of the experimental setup are shown in Figs. 4 and 5, respectively. Experiments are performed in the quadrantal enclosure consisting of two isothermal walls and an insulated nonconducting wall. The adiabatic wall of the quadrantal test section is made of 10 mm thick Plexiglass material with an inside radius of 30 mm, which is used due to its transparency, good optical properties, and low thermal conductivity (0.19 W/m K). The heat transfer surfaces of the enclosure consist of 10 mm thick copper plates having dimensions of 30 mm width for the hot bottom wall, 30 mm height for the cold vertical wall, and 60 mm depth for both surfaces. The copper plates were highly polished in order to reduce emissivity (e=0.03) and, following that, radiative heat transfer. The excellent thermal capacity and thermal conductivity of copper surfaces lead us to consider heated and cooled walls at uniform and constant temperatures. The test cell used in the present study was constructed in order to provide the required range of Rayleigh number values. Each heat transfer surface of the test section is connected to a thermostatic bath so as to keep the surfaces at a prescribed uniform temperature. For each pair of heaters, the flow rate is supplied at the same level. The pipes of the thermostatic circuit were covered with rubber foam to prevent heat losses. The test section was filled with distilled water with a hole located at top rear side of the cell, which is sealed by a designed screw system made from Plexiglas material with an o-ring. The filling process was employed with a syringe and a thin needle in order to avoid air bubbles. The operating conditions of the experiments are shown in Table 2. In the table, it can be seen that the maximum temperature difference in the experiments between the hot and cold walls is 17.4 K, and this temperature range is in the limit that Boussinesq approximation can be used [15].

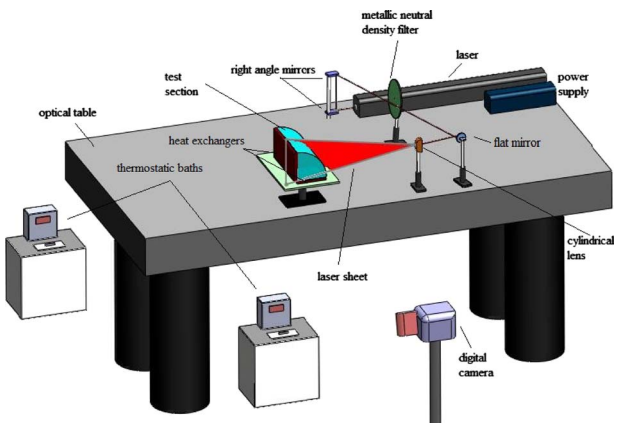

Fig. 5 Schematic picture of the experimental facility with optical installation

Table 2 Experimental conditions

Experiment	Ra	ΔT (K)	Pr	Cavity size (m)
Expt. 1	1.7×10^5	0.4	6.62	0.03
Expt. 2	10^6	2.4	6.62	0.03
Expt. 3	5×10^6	11.4	6.62	0.03
Expt. 4	10^7	17.4	5.83	0.03

Three 0.4 mm diameter copper/constantan thermocouples were installed along the centerline of each of the two heated and cooled walls. The thermocouples were inserted 5 mm under the copper plates, and the distance among them was 7.5 mm. In order to obtain temperature measurements, all thermocouples were connected to a digital data logger, and therefore surface temperatures of the walls were controlled. The maximum temperature variation from the average temperature of the heat transfer surfaces was ±0.2 K, and the precision of measurements was ±0.1 K. Once all parts of the experimental setup were assembled, it was insulated with 10 mm thick rubber-plastic foam heat insulation material.

At the beginning of each experiment, the ambient temperature was controlled and kept constant at 22°C and 50% relative humidity by air-conditioners. At the initial state of the experiments, thermostatic bath units were switched on and set to the hot and cold wall temperatures, and the laser was opened to become stable. When the conditions were found to be in thermal equilibrium, the test cell was filled with distilled water with the seeding material. The seeding used was 10 μm diameter hollow glass spheres (HGSs) with 1.1 g/cm^3 density. To make sure of the seeding material to trace, the fluid motion that the methodology described in Merzkirch [16] was used. The sedimentation velocity of a spherical particle is given by

$$v_s = (g d_p^2 / 18 \upsilon_f)\{(\rho_p/\rho_f) - 1\} \tag{21}$$

where g is the gravitational acceleration. A particle is neutrally buoyant if $v_s \cong 0$. Since the condition $\rho_p/\rho_f \cong 1$ cannot be always fulfilled, neutral buoyancy can also be approached by using extremely small (i.e., micron-sized) particles [16]. In our study, v_s is equal to 5.67×10^{-6}. The visualization was made by means of a laser sheet generated by a 35 mW He–Ne laser source with a 632.8 nm wavelength. The laser sheet was generated by an optical installation. The density of the laser beam was controlled by a metallic neutral density filter, and the beam was collimated by flat and right angle mirrors. After that, the laser beam was transformed into a sheet of light by passing through a plano-convex cylindrical lens made of BK7 material having a 12.7 mm focus length. The light sheet enters through the middle of the curved adiabatic wall made of Plexiglas and illuminates the middle cross-section of the cavity. The laser sheet was prevented to reach the enclosure by a shutter and was only disclosed during the flow visualization times in order to avoid laser light to heat the fluid inside the enclosure. A digital camera was located perpendicular to the laser sheet to acquire the images of the flow field with 25 frames/s.

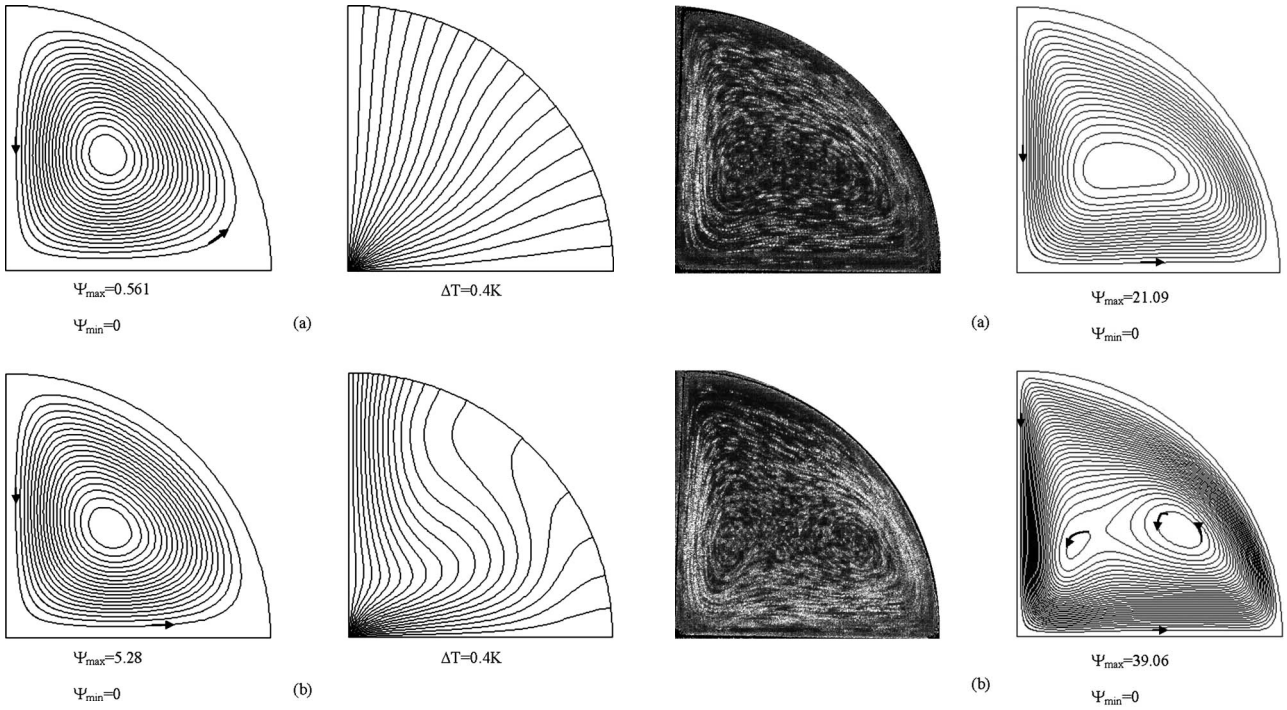

Fig. 6 Streamlines (left) and isotherms (right) for (*a*) Ra=10^3 and (*b*) Ra=10^4

4 Results and Discussion

In this paper, natural convection in an enclosure heated and cooled on adjacent walls given in Fig. 1 is studied experimentally and numerically. Mainly, the effects of the Rayleigh number, Ra, on the heat transfer as well as flow and temperature fields are investigated. The experimental study covers four different values of Ra (Ra=1.7×10^5, 10^6, 5×10^6, and 10^7), while the numerical study is in a broader range of Ra. These Ra number ranges are selected in order to examine the Ra effects in the laminar regime range.

Figure 6 shows streamlines and isotherms obtained numerically for Ra=10^3 and Ra=10^4, respectively. For Ra=10^3, the isotherms present a nearly diagonally symmetrical structure, which is very similar to those obtained for the conduction regime (see Fig. 3). Because of the geometrical and boundary condition similarity of the problem studied with that studied by Aydin et al. [3], increasing Ra presented very similar results. Therefore, we refer the reader to that paper for an in-depth discussion of the physics of the problem. Increasing Ra will increase the dominancy of the convection on the transport. For Ra=10^3, streamlines form a nearly centrally located single cell, and corresponding isotherms exhibit the characteristics of pure conduction forming a diagonally symmetric structure, as illustrated in Fig. 6(*a*). The hot fluid layer heated around the hot wall ascends upward by reason of decreasing density and the weak circulation in the enclosure. On the other hand, nearby the cold wall, the fluid layer with increased density moving downward sweeps the hot fluid layer forward. These mutual effects of the hot and cold fluid layers cause isotherms to widen. As the Rayleigh number increases (Ra=10^4), the general structure of the streamlines does not deteriorate, but this interaction becomes stronger, and the center of the cell moves toward the lower right corner of the enclosure by forming an elliptical shape.

Figures 7 and 8 demonstrate the experimental and numerical streamlines and numerical isotherms, respectively, for higher values of Ra. At Ra=1.7×10^5, recirculation intensity increases to a degree that boundary layer formations are observed adjacent to the heated and cooled walls. This situation can be distinctly seen through the experimental results, too. Further increases in Ra from

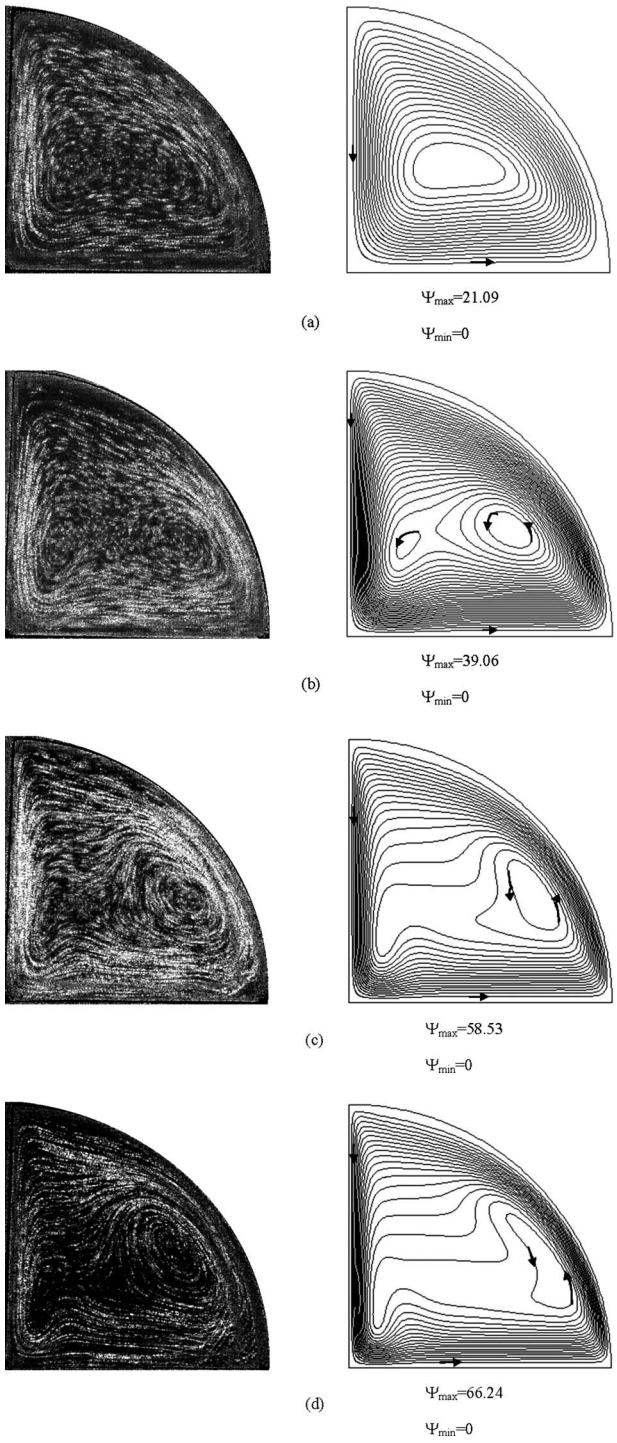

Fig. 7 Experimental (left) and numerical (right) streamlines: (*a*) Ra=1.7×10^5, (*b*) Ra=10^6, (*c*) Ra=5×10^6, and (*d*) Ra=10^7

1.7×10^5 to 10^6, 5×10^6, and 10^7 result in distinct boundary layers, and as a consequence, the energy transport is enhanced. As can be seen from Figs. 7 and 8, at higher Rayleigh numbers, Ra $\geq10^6$, boundary layers on the hot and cold walls are observed from the corresponding experimental and numerical streamlines and isotherms obtained numerically. An instability that may arise from the vertical temperature gradient due to the hot bottom wall is unlikely because of the suppression effect of the descending cold fluid layer along the cold wall [4]. Owing to this suppression effect, secondary and tertiary circulations of warmer fluid are observed for Ra=10^6, 5×10^6, and 10^7 (see Fig. 7). A tertiary circu-

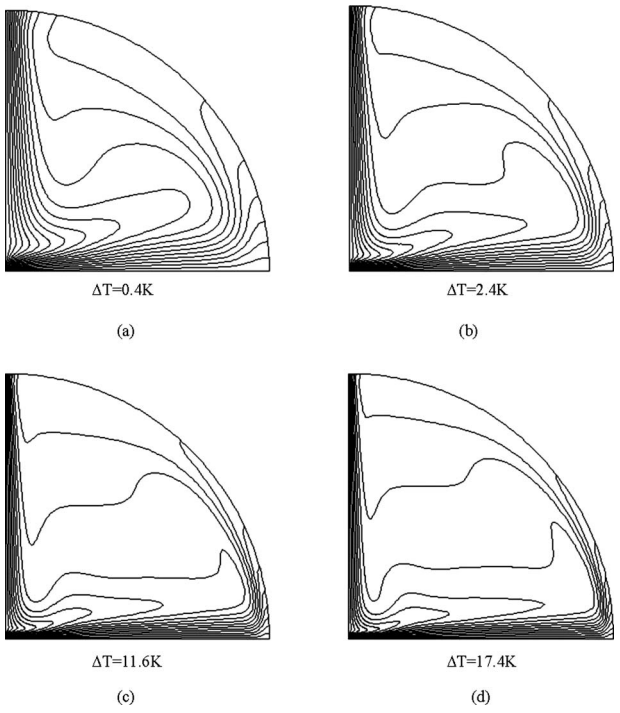

Fig. 8 Numerical isotherms: (*a*) Ra=1.7×10^5, (*b*) Ra=10^6, (*c*) Ra=5×10^6, and (*d*) Ra=10^7

lation is observed only for Ra=10^6, which diminishes as Ra increases to 5×10^6 and 10^7. On the other hand, secondary flows are also a result of the elliptical shape of the central roll cell structure. As mentioned above, for Ra≤10^4, the central roll cell is a nearly circular form, and the isotherms exhibit nearly pure conduction distribution. As Ra is increased to 10^4, convective motion becomes dominant and circular cell motion returns to an elliptical shape. Further increase in Ra distorts this elliptical structure by separating it into secondary cells. Moreover, existing thermal stratification is examined in view of studies of Angirasa and Srinivasan [17] and Mallik et al. [18]. It is reported by Angirasa and Srinivasan [17] that as thermal stratification increases, the local buoyancy force is depleted and the vertical velocity levels fall. The flow reverses in the outer region of the boundary layer because of the temperature defect. In this case, it is seen that the enclosure induces stratification of the thermal field away from the boundary layers. From Ra=5×10^6 to 10^7, a secondary cell gets close to the curved adiabatic wall with an extension and elongation.

The effect of Ra on the average Nusselt number is demonstrated in Fig. 9, while the local Nusselt number variation with Ra is shown in Fig. 10. At low Rayleigh numbers (Ra≤10^4), the influence of Rayleigh number on the average Nusselt number is not significant. The influence becomes stronger as the Rayleigh number increases beyond 10^4. The poor heat transfer performance at low Ra numbers can be attributed to the weaker convection.

From Figs. 9 and 10, it can be seen that the discontinuity points near the adjacent hot and cold walls are overcome by the calculation procedure of the Nusselt number suggested. The Nusselt number slightly increases around the corner point and continues to increase along the hot wall in order that temperature difference between the hot wall and the adjacent fluid layer decreases along the r-direction. In the same figures, for comparison purposes of conduction dominated and convection dominated regimes, Nusselt numbers are plotted from Ra=10^3 to 10^7. For Ra=10^3, the numerical result of the Nusselt number is equal to 1; this result agrees well with the analytical solution and exhibits conduction characteristics.

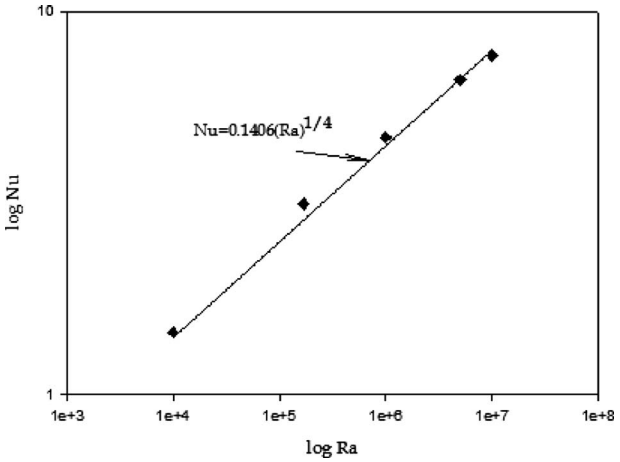

Fig. 9 Average Nusselt number on the heated wall versus Rayleigh number

The Nu–Ra relation follows the power law Nu∼Ra$^{1/4}$ approximately beyond Ra=10^4. Based on the numerical results obtained in this paper, a correlation equation can establish the dependence of Nu on Ra as follows:

$$\mathrm{Nu} = 0.1406(\mathrm{Ra})^{1/4} \tag{22}$$

The minimum and maximum errors between the results obtained with the correlation and numerical solutions by Eq. (22) are 0.27% and 9.15%, respectively. Figure 9 also shows the deviation of the Nusselt number between the correlation and the numerical prediction.

5 Concluding Remarks

In this paper, an experimental and numerical study has been carried out for buoyancy-driven flow and heat transfer in a two-dimensional quadrantal enclosure isothermally heated from the bottom and cooled from the vertical side. The influence of Rayleigh number on convective heat transfer and flow structure is examined in the range of 10^3≤Ra≤10^7. Flow visualization experiments have enabled us to observe the flow pattern in the enclosure, which has also enabled us to explain the convection phenomenon and to compare the numerical predictions. Up to Ra =10^6, a single central-cell structure has been observed in the enclosure. However, the shape of the cell has turned into an elliptical as Ra increases. Due to the distortion of this elliptical shape, sec-

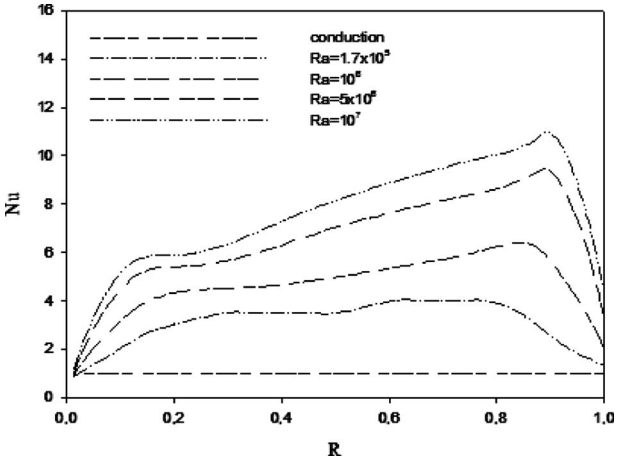

Fig. 10 Local Nusselt number on the heated wall versus Rayleigh number

ondary flows for $Ra=5\times10^6$ and 10^7 and tertiary flows for $Ra=10^6$ have been observed. A new methodology for the calculation of Nu has been suggested to overcome the singularity dependence of Nu near the intersection of the differentially heated isothermal adjacent walls, which has been proved to work very well.

Acknowledgment

The first author (O.A.) of this paper is also indebted to the Turkish Academy of Sciences (TUBA) for the financial support provided under the Programme to Reward Success Young Scientists (TUBA-GEBIT).

Nomenclature

- Ra = Rayleigh number, $g\beta(T_h-T_c)H^3/(\upsilon\alpha)$
- Nu = Nusselt number
- T = temperature
- Pr = Prandtl number
- H = enclosure height
- e = emissivity
- p = pressure
- P = nondimensional pressure
- k = thermal conductivity
- h = convective heat transfer coefficient
- q = heat flux
- c_p = specific heat
- u = velocity component in the x-direction
- v = velocity component in the v-direction
- U = nondimensional velocity component in the x-direction
- V = nondimensional velocity component in the y-direction
- x,y = Cartesian coordinate system
- X,Y = nondimensional coordinates
- r,ϕ = cylindrical coordinate system
- R = dimensionless length of the hot wall, r/H

Greek Symbols

- Ψ = nondimensional stream function $(=\psi/\alpha)$
- ψ = stream function
- ρ = density
- β = coefficient of thermal expansion
- υ = kinematic viscosity
- α = thermal diffusivity
- μ = dynamic viscosity
- θ = dimensionless temperature

Subscripts

- h = hot wall
- c = cold wall
- max = maximum
- min = minimum

References

[1] November, M., and Nansteel, M. W., 1987, "Natural Convection in Rectangular Enclosures Heated From Below and Cooled Along One Side," Int. J. Heat Mass Transfer, **30**, pp. 2433–2440.

[2] Ganzarolli, M. M., and Milanez, L. F., 1995, "Natural Convection in Rectangular Enclosures Heated From Below and Symmetrically Cooled from Sides," Int. J. Heat Mass Transfer, **38**, pp. 1063–1073.

[3] Aydin, O., Ünal, A., and Ayhan, T., 1999, "Natural Convection in Rectangular Enclosures Heated From One Side and Cooled From the Ceiling," Int. J. Heat Mass Transfer, **42**, pp. 2345–2355.

[4] Aydin, O., Ünal, A., and Ayhan, T., 1999, "A Numerical Study on Buoyancy-Driven Flow in an Inclined Square Enclosure Heated and Cooled on Adjacent Walls," Numer. Heat Transfer, Part A, **36**, pp. 585–599.

[5] Aydin, O., and Yang, W. J., 2000, "Natural Convection in Enclosures With Localized Heating From Below and Symmetrical Cooling From Sides," Int. J. Numer. Methods Heat Fluid Flow, **10**, pp. 518–529.

[6] Angirasa, D., Chinnakotla, R. B., and Mahajan, R. L., 1994, "Buoyancy-Induced Convection From Isothermal L-Shaped Corners With Symmetrically Heated Surfaces," Int. J. Heat Mass Transfer, **37**, pp. 2439–2463.

[7] Chinnakotla, R. B., Angirasa, D., and Mahajan, R. L., 1996, "Parametric Study of Buoyancy-Induced Flow and Heat Transfer From L-Shaped Corners With Asymmetrically Heated Surfaces," Int. J. Heat Mass Transfer, **39**, pp. 851–865.

[8] Angirasa, D., and Mahajan, R. L., 1993, "Natural Convection From L-Shaped Corners With Adiabatic and Cold Isothermal Horizontal Walls," ASME J. Heat Transfer, **115**, pp. 149–157.

[9] Corvaro, F., and Paroncini, M., 2007, "Experimental Analysis of Natural Convection in Square Cavities Heated From Below With 2D-PIV and Holographic Interferometry Techniques," Exp. Therm. Fluid Sci., **31**, pp. 721–739.

[10] Ishihara, R., Fukui, T., and Matsumoto, R., 2002, "Natural Convection a Vertical Rectangular Enclosure With Localized Heating and Cooling Zones," Int. J. Heat Fluid Flow, **23**, pp. 366–372.

[11] Shiina, Y., Fujimura, K., Kunugi, T., and Akino, N., 1994, "Natural Convection in a Hemispherical Enclosure Heated From Below," Int. J. Heat Mass Transfer, **37**, pp. 1605–1617.

[12] Chen, C. L., and Cheng, C. H., 2002, "Buoyancy-Induced Flow and Convective Heat Transfer in an Inclined Arc-Shaped Enclosure," Int. J. Heat Fluid Flow, **23**, pp. 823–830.

[13] Kim, H. S., Kim, C. J., and Ro, S. T., 1996, "Heat Transfer Correlation for Natural Convection in a Meniscus-Shaped Cavity and Its Application to Contact Melting Process," Int. J. Heat Mass Transfer, **39**, pp. 2267–2270.

[14] FLUENT User's Guide, Release 6.3.26, Fluent Incorporated (2005-01-06).

[15] Valencia, L., Pallares, J., Cuesta, I., and Grau, F. X., 2005, "Rayleigh-Bénard Convection of Water in a Perfectly Conducting Cubical Cavity: Effects of Temperature-Dependent Physical Properties in Laminar and Turbulent Regimes," Numer. Heat Transfer, Part A, **47**(4), pp. 333–352.

[16] Merzkirch, W., 1987, *Flow Visualization*, 2nd ed., Academic, Orlando, pp. 38–48.

[17] Angirasa, D., and Srinivasan, J., 1992, "Natural Convection Heat Transfer From an Isothermal Vertical Surface to a Stable Thermally Stratified Fluid," ASME J. Heat Transfer, **114**, pp. 917–923.

[18] Mallik, S., Angirasa, D., and Mahalingam, S., 1998, "Limitation of Boundary Layer Analyses for Buoyant Convection in Stably Stratified Fluids," Numer. Heat Transfer, Part A, **34**, pp. 617–631.